

## Photonic crystal slab quantum well infrared photodetector

S. Kalchmair,<sup>1,a)</sup> H. Detz,<sup>1</sup> G. D. Cole,<sup>2</sup> A. M. Andrews,<sup>1</sup> P. Klang,<sup>1</sup> M. Nobile,<sup>1</sup> R. Gansch,<sup>1</sup> C. Ostermaier,<sup>1</sup> W. Schrenk,<sup>1</sup> and G. Strasser<sup>1,3</sup>

<sup>1</sup>Center for Micro- and Nanostructures, Vienna University of Technology, Floragasse 7, 1040 Wien, Austria

<sup>2</sup>Faculty of Physics, University of Vienna, Boltzmannngasse 5, 1090 Vienna, Austria

<sup>3</sup>Department of Electrical Engineering and Department of Physics, The State University of New York at Buffalo, 332 Bonner Hall, Buffalo, New York 14260-1920, USA

(Received 25 August 2010; accepted 20 December 2010; published online 4 January 2011)

In this letter we present a quantum well infrared photodetector (QWIP), which is fabricated as a photonic crystal slab (PCS). With the PCS it is possible to enhance the absorption efficiency by increasing photon lifetime in the detector active region. To understand the optical properties of the device we simulate the PCS photonic band structure, which differs significantly from a real two-dimensional photonic crystal. By fabricating a PCS-QWIP with 100x less quantum well doping, compared to a standard QWIP, we are able to see strong absorption enhancement and sharp resonance peaks up to temperatures of 170 K. © 2011 American Institute of Physics.

[doi:10.1063/1.3537954]

Research on photonic crystals (PCs), structures with a periodic refractive index modulation, has opened up several avenues for the control of light.<sup>1,2</sup> Most existing devices are realized as two-dimensional (2D) PC structures, as they are compatible with standard semiconductor processing.<sup>3-6</sup> An important class of 2D-PC structures is the photonic crystal slabs (PCSs). The PCS is a dielectric structure with a periodic index modulation in only two dimensions and refractive index guiding in the third.<sup>7-9</sup> The applications for PCSs range from optical resonators<sup>10</sup> to lasers<sup>11,12</sup> and detectors.<sup>13,14</sup>

In this letter, we present a quantum well infrared photodetector (QWIP) fabricated as a PCS structure. Extensive research has been conducted on QWIPs, which are now a commercially viable technology.<sup>15-17</sup> One important application is thermal imaging with focal plane arrays.<sup>18</sup> However, to achieve high signal-to-noise ratios most systems need to be operated at liquid nitrogen temperatures. The PCS-QWIP structure, presented in this letter, could provide a way to improve temperature performance of QWIPs by resonant absorption enhancement. Here we investigate the optical properties of a PCS-QWIP and compare it to standard QWIP devices.

The QWIPs are grown by molecular beam epitaxy as a GaAs/Al<sub>0.30</sub>Ga<sub>0.70</sub>As bound-to-quasibound structure, designed to operate at a wavelength of 8 μm. The active region consists of 26 periods, each with a well and barrier width of  $w=4.5$  nm and  $b=45$  nm, respectively. Two different QWIP designs are used: One doped with an equivalent sheet carrier density of  $4 \times 10^{11}$  cm<sup>-2</sup>, grown on semi-insulating GaAs substrate, and a low doped with  $4 \times 10^9$  cm<sup>-2</sup> sheet carrier density, grown on n+GaAs substrate. The highly doped QWIP is used as the reference material. Following the design guidelines for an optimized detector in Ref. 17, the optimum detectivity is expected around  $T=100$  K for this doping density. The doping level of the low doped QWIP is chosen to be far below the optimum, which results in much smaller absorption efficiency. The

QWIP layer sequence is a GaAs substrate, followed by a 2 μm thick Al<sub>0.85</sub>Ga<sub>0.15</sub>As sacrificial layer, a 500-nm-thick GaAs ( $2 \times 10^{18}$  cm<sup>-3</sup>) bottom contact layer, the 1.4 μm thick active region, and a 100 nm GaAs ( $2 \times 10^{18}$  cm<sup>-3</sup>) top contact layer.

From each QWIP detector material, PCS-QWIPs and, for comparison, standard mesa QWIPs are fabricated. The PC structures are underetched by selectively removing the sacrificial AlGaAs layer with a 24% HCl solution to create the free standing PCSs [Fig. 1(a)]. A schematic illustration of the finished device is shown in Fig. 1(b). The spectral response of the standard QWIP has a peak at 1250 cm<sup>-1</sup> (Fig. 2, dashed line). Light below this frequency does not have sufficient energy to excite electrons from the bound state to the continuum. For photons above this frequency an electronic transition becomes more unlikely, hence the absorption is reduced.

The photocurrent spectrum of the PCS-QWIP (Fig. 2, solid line) also shows a response peak at 1250 cm<sup>-1</sup>, but additionally displays several pronounced resonance peaks.

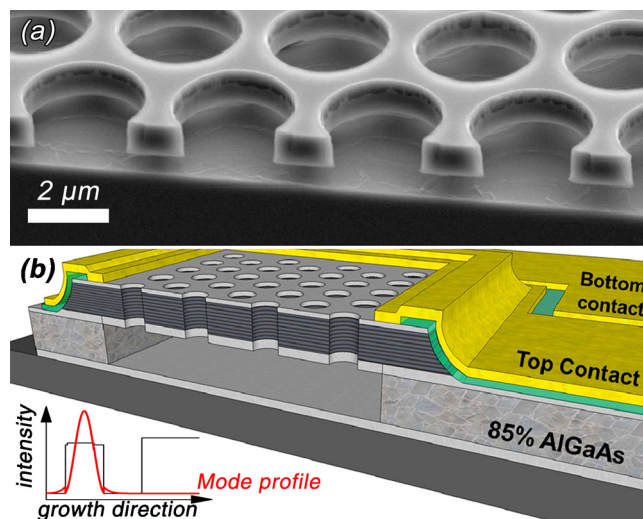


FIG. 1. (Color online) PCS-QWIP design. (a) SEM image of a cleaved PCS. (b) Cross section through the PCS-QWIP structure.

<sup>a)</sup>Electronic mail: stefan.kalchmair@tuwien.ac.at.

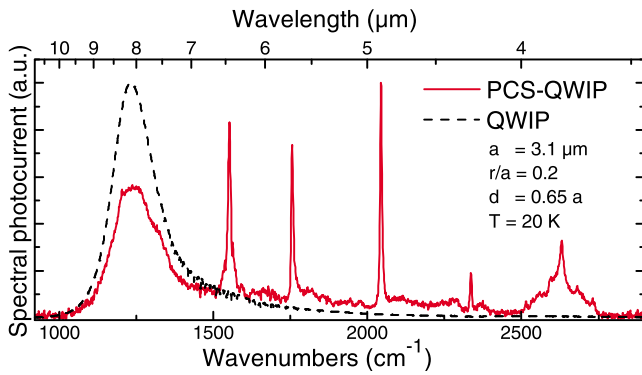


FIG. 2. (Color online) Normalized photocurrent spectra of a PCS-QWIP (solid line) at surface normal incidence and a standard QWIP (dashed line) at  $45^\circ$  wedged illumination. PC parameters are  $a=3.1 \mu\text{m}$ ,  $r/a=0.2$  and slab thickness  $d=0.65 a$ .

To describe the effect of the PC in a PCS-QWIP, we can split the response into two separate functions: (1) coupling of the external field into a PCS mode and (2) resonant absorption enhancement. Without a PC, the device would be insensitive to surface normal incidence illumination as an electronic transition in the QWIP requires an electric field perpendicular to the quantum wells.<sup>17</sup> For this reason, without an additional coupling mechanism, the standard QWIP is always measured at a  $45^\circ$  angle of illumination. In most commercially available QWIP devices, the coupling of the incoming radiation is achieved by fabricating a grating onto the QWIP surface.<sup>19,20</sup> In contrast to a grating, the PCS not only allows coupling to normal incidence radiation, but also acts as a resonator, which increases the photon lifetime in the active region of the QWIP and, thereby, enhances the absorption efficiency. Each of the sharp peaks in Fig. 2 corresponds to an excited PCS resonance.

The optical properties of PC structures are represented by the photonic band structure. It was calculated for the PCS, shown in Fig. 2, by the revised plane wave expansion method (Fig. 3).<sup>21</sup> All dimensions used in the simulation were extracted from SEM measurements. The band structure of a PCS significantly differs from a 2D-PC, which theoretically extends to infinity in the out-of-plane direction.<sup>7</sup> The leaking of the modes out of the slab causes the photonic

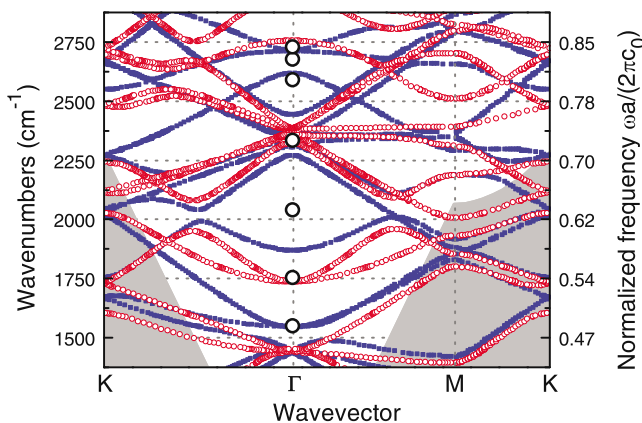


FIG. 3. (Color online) Photonic band structure of a PCS. The photonic modes have odd (blue squares) or even (open red circles) symmetry. The measured PCS resonances (large open circles) correspond to excited PCS modes. The gray area marks guided modes, which cannot couple to external waves.

bands to shift toward higher frequencies with respect to a 2D-PC. The shift depends of the mode symmetry; odd modes are shifting stronger than even modes.

In a 2D-PC the modes split into transverse electric (TE) and transverse magnetic (TM) polarizations. A QWIP in a real 2D-PC would only detect TM modes, as the TE modes have no electric field in growth direction. The modes in a PCS show even or odd mode symmetry with respect to the mirror plane in the slab center, but are not purely TE or TM anymore.<sup>22</sup> Further, polarization mixing can transfer energy from one mode to another.<sup>23</sup> For this reason odd and even modes can be detected by the QWIP (Fig. 3).

The measured resonance peaks in the photocurrent spectrum (Fig. 2) can be explained with the simulated photonic band structure (Fig. 3). The measurement was performed at surface normal incidence, so the in-plane wave vector is zero ( $\Gamma$ -point). The frequencies of the lowest two resonances coincide very well with the simulated photonic bands. The third resonance falls right between the photonic bands, it most likely corresponds to a higher order slab mode. In this simulation only first order slab modes were calculated. All other resonance peaks correspond to higher photonic bands. The simulated values deviate from the measurements for higher modes, where the simulation is more sensitive to small changes of the device geometry or refractive indices. The fact that some PCS modes are seen as resonance peaks while others are invisible can be explained by symmetry arguments. A pronounced resonance peak is only visible when the PCS mode is in-plane symmetry-matched to an incident wave.<sup>22</sup>

The widths of the resonance peaks (Fig. 2) depend on the photon lifetime in the resonator and are determined by the decay rate of the electromagnetic energy in the corresponding PCS eigenmode. A useful measure for the photon lifetime is the quality factor  $Q$ , defined as  $\omega/\delta\omega$ . In the lateral direction, the flow of the electromagnetic energy is described by the group velocity  $v_g$ , which is given by the slope of the photonic bands in the photonic band structure. At the  $\Gamma$ -point (normal incidence), the bands are flat,  $v_g$  is very small and the  $Q$ -factor can be large. For the third resonance peak in Fig. 2 we measured  $Q=295$ . In the out-of-plane direction, the light is confined by the high refractive index contrast between slab and surrounding air, which is a significant advantage of the PCS design.

The increased photon lifetime leads to absorption enhancement in the active region. By designing a PCS to have a resonance at the QWIP absorption peak, the photocurrent can be increased while thermally generated dark current remains constant (Fig. 4). In the high doped QWIP material, however, the absorption is already high and the resonant enhancement is small (upper two lines in Fig. 4). For this reason the low doped QWIP material was grown. By reducing the quantum well doping, the absorption efficiency and the dark current are reduced simultaneously. Now, the PCS resonance can develop and enhance the low QWIP absorption. The comparison of a PCS-QWIP to a standard QWIP with  $100\times$  less doping shows a pronounced resonance peak right at the QWIP peak absorption at  $1315 \text{ cm}^{-1}$  ( $8.4 \mu\text{m}$ ). A direct comparison of the peak width for this resonance peak for high and low doping is shown in the inset in Fig. 4.

As the low doped standard QWIP is grown on  $n$ -GaAs substrate and illuminated at a  $45^\circ$  angle from the

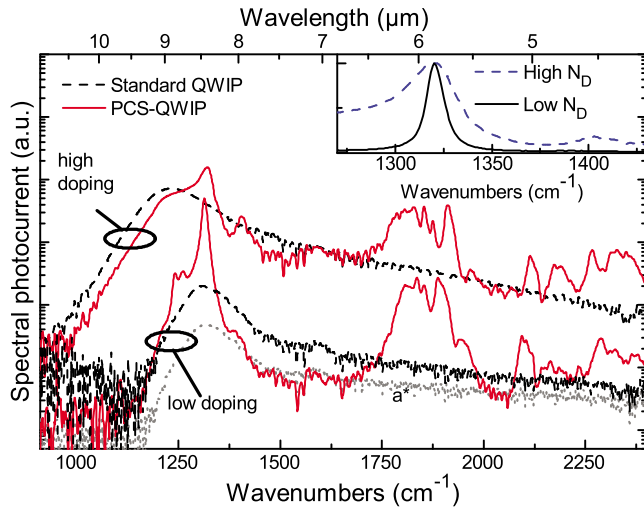


FIG. 4. (Color online) Photocurrent response of a standard QWIP (dashed line) and a PCS-QWIP (solid line). The PC parameters are  $a=4 \mu\text{m}$ ,  $r/a=0.2$ ,  $d=0.65 a$ , temperature is 70 K. The device with high doping (upper two lines) shows only weak absorption enhancement and a broad resonance peak at  $1315 \text{ cm}^{-1}$ , while the low doped device (lower two lines) shows strong resonant enhancement. The low doped standard QWIP spectrum (lower dashed line) was divided by the  $n+$  substrate transmission to compensate for absorption losses. The original measurement data is shown as dotted line ( $a^*$ ). Inset: comparison of the normalized PCS resonance peaks. For high doping (dashed line), the Q-factor  $Q_{\text{HD}}=28$ , for low doping (solid line)  $Q_{\text{LD}}=125$ .

backside, the light is partly absorbed by free carrier absorption. To compensate for this additional absorption, the photocurrent response of the standard QWIP is divided by the calculated substrate transmission. From the first resonance peak at  $1315 \text{ cm}^{-1}$  to the higher resonances around  $1850 \text{ cm}^{-1}$  the transmission is in the range from 20% to 40%.

At higher temperatures, the performance of QWIPs is usually limited by thermally generated dark current, which depends exponentially on the doping density.<sup>17</sup> However, in standard QWIPs a high doping density is required to achieve strong absorption. In the PCS-QWIP the absorption is resonantly enhanced without creating additional dark current [Fig. 5(a)]. At low temperatures ( $<70 \text{ K}$ ), the dark current is dominated by background blackbody radiation, therefore it is constant [Fig. 5(b)]. At higher temperatures the dark current grows exponentially and the photocurrent signal is covered

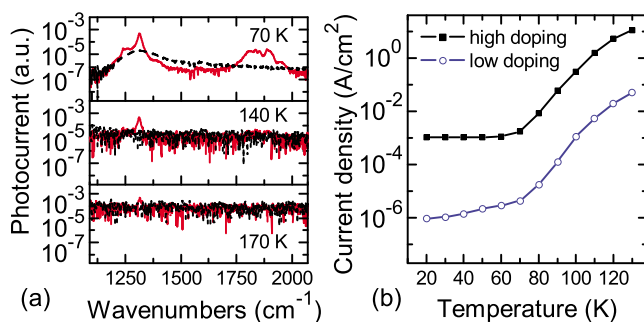


FIG. 5. (Color online) Temperature performance. (a) Temperature dependent photocurrent spectra of a PCS-QWIP (solid red line) and a standard QWIP (dashed black line) with low doping. At higher temperatures, the standard QWIP signal disappears in the noise, while the PCS-QWIP signal is still visible. (b) Comparison of the dark current densities of a high and a low doped QWIP.

in the background noise. The standard QWIP signal vanishes in the noise before 140 K while the PCS-QWIP resonance is still visible at 170 K [Fig. 5(a)]. At even higher temperatures it is not possible to operate the QWIPs, as the signal vanishes in the dark current and the high current density starts heating the QWIP.

In conclusion, we presented a QWIP, which is fabricated as a PCS structure. With the PCS it is possible to resonantly enhance the absorption in the detector active region. To understand the optical properties of the device we simulated the photonic band structure, which differs significantly from a real 2D-PC. Accurate results are received only if the influence of the slab guiding is considered. By fabricating a PCS-QWIP with low quantum well doping, we were able to see strong absorption enhancement. The sharp resonance peaks were visible at temperatures up to 170 K. Further research on this topic will include optimization of the PCS, as Q-factors of several thousand have been theoretically predicted. For narrow band signals the PCS-QWIP design should allow to build detectors with improved detectivity. We envision that this approach will enable significant improvement in QWIP detector performance for industrial applications including thermal imaging or high speed data transmission.

The authors acknowledge the support by the Austrian FWF project IRON (SFB-25-03), the PLATON (V01101-08-BI) project within the Austrian NANO Initiative and the “Gesellschaft für Mikro- und Nanoelektronik” GMe. G.D.C. is a recipient of a Marie Curie Fellowship of the European Commission (EC).

- <sup>1</sup>E. Yablonovitch, *Phys. Rev. Lett.* **58**, 2059 (1987).
- <sup>2</sup>J. D. Joannopoulos, P. R. Villeneuve, and S. Fan, *Nature (London)* **386**, 143 (1997).
- <sup>3</sup>O. Painter, R. K. Lee, A. Scherer, A. Yariv, J. D. O’Brien, P. D. Dapkus, and I. Kim, *Science* **284**, 1819 (1999).
- <sup>4</sup>S. Scharfner, S. Golka, C. Pflügl, W. Schrenk, A. M. Andrews, T. Roch, and G. Strasser, *Appl. Phys. Lett.* **89**, 151107 (2006).
- <sup>5</sup>S. Scharfner, S. Kalchmair, A. M. Andrews, P. Klang, W. Schrenk, and G. Strasser, *Appl. Phys. Lett.* **94**, 231117 (2009).
- <sup>6</sup>A. Benz, C. Deutsch, G. Fasching, K. Unterrainer, A. Andrews, P. Klang, W. Schrenk, and G. Strasser, *Opt. Express* **17**, 941 (2009).
- <sup>7</sup>S. Fan and J. D. Joannopoulos, *Phys. Rev. B* **65**, 235112 (2002).
- <sup>8</sup>S. G. Johnson, S. Fan, P. R. Villeneuve, J. D. Joannopoulos, and L. A. Kolodziejski, *Phys. Rev. B* **60**, 5751 (1999).
- <sup>9</sup>K. Inoue, N. Kawai, Y. Sugimoto, N. Carlsson, N. Ikeda, and K. Asakawa, *Phys. Rev. B* **65**, 121308 (2002).
- <sup>10</sup>M. Kaniber, A. Kress, A. Laucht, M. Bichler, R. Meyer, M.-C. Amann, and J. J. Finley, *Appl. Phys. Lett.* **91**, 061106 (2007).
- <sup>11</sup>H. Y. Ryu, H. G. Park, and Y. H. Lee, *IEEE J. Sel. Top. Quantum Electron.* **8**, 891 (2002).
- <sup>12</sup>S. Noda, M. Fujita, and T. Asano, *Nat. Photonics* **1**, 449 (2007).
- <sup>13</sup>J. Yang, M. Seo, I. Hwang, S. Kim, and Y. Lee, *Appl. Phys. Lett.* **93**, 211103 (2008).
- <sup>14</sup>W. Suh, M. F. Yanik, O. Solgaard, and S. Fan, *Appl. Phys. Lett.* **82**, 1999 (2003).
- <sup>15</sup>B. F. Levine, *J. Appl. Phys.* **74**, R1 (1993).
- <sup>16</sup>A. Rogalski, *J. Appl. Phys.* **93**, 4355 (2003).
- <sup>17</sup>H. Schneider and H. C. Liu, *Quantum Well Infrared Photodetectors* (Springer, Berlin, 2007).
- <sup>18</sup>S. D. Gunapala, S. V. Bandara, J. K. Liu, J. M. Mumolo, D. Z. Ting, C. J. Hill, and J. Nguyen, *Sensors, 2009 IEEE* **2009**, 1609 (2009).
- <sup>19</sup>J. Y. Andersson, L. Lundqvist, and Z. F. Paska, *Appl. Phys. Lett.* **58**, 2264 (1991).
- <sup>20</sup>Y. Fu, M. Willander, W. Lu, and W. Xu, *J. Appl. Phys.* **84**, 5750 (1998).
- <sup>21</sup>S. Shi, C. Chen, and D. W. Prather, *Appl. Phys. Lett.* **86**, 043104 (2005).
- <sup>22</sup>T. Ochiai and K. Sakoda, *Phys. Rev. B* **63**, 125107 (2001).
- <sup>23</sup>V. N. Astratov, D. M. Whittaker, I. S. Culshaw, R. M. Stevenson, M. S. Skolnick, T. F. Krauss, and R. M. De La Rue, *Phys. Rev. B* **60**, R16255 (1999).